International Journal of Fluid Machinery and Systems
Vol. 9, No. 2, April-June 2016
DOI: http://dx.doi.org/10.5293/IJFMS.2016.9.2.160
ISSN (Online): 1882-9554

Original Paper

Dynamic Response of Blade Surface Cavitation

Masakazu Toyoshima[1], Kimiya Sakaguchi[1], Kota Tsubouchi[1],

Hironori Horiguchi[1] and Kazuyasu Sugiyama[1]

[1]Graduate School of Engineering Science, Osaka University
1-3 Machikaneyama, Toyonaka, Osaka 560-8531, Japan,
masakazu.toyoshima@flow.me.es.osaka-u.ac.jp, kimiya.sakaguchi@flow.me.es.osaka-u.ac.jp,
kota.tsubouchi@flow.me.es.osaka-u.ac.jp, horiguti@me.es.osaka-u.ac.jp,
kazuyasu.sugiyama@me.es.osaka-u.ac.jp

Abstract

In high speed turbopumps, cavitation occurs and often causes the flow instabilities such as cavitation surge and rotating cavitation. The occurrence of these cavitation instabilities is considered to relate to dynamic characteristics of the cavitation, which are modelled using a cavitation compliance and a mass flow gain factor. Various types of cavitation such as a blade surface cavitation, a tip leakage vortex cavitation, and a backflow vortex cavitation occur at the same time in the inducer and the dynamic characteristics of each cavitation have not been clarified yet in experiments. Focusing on the blade surface cavitation as one of fundamental cavitation, we investigated the dynamic characteristics of the blade surface cavitation on a flat plate hydrofoil in experiments in the present study.

Keywords: Cavitation, Hydrofoil, Dynamic Characteristics, Experiment

1. Introduction

In high speed turbopumps, cavitation occurs and often causes flow instabilities such as cavitation surge [1, 2] and rotating cavitation [3, 4]. The occurrence of these cavitation instabilities is considered to relate to dynamic characteristics of cavitation [5], which are modelled as a cavitation compliance and a mass flow gain factor [6]. The cavitation compliance K is a rate of change in cavity volume for a change in suction pressure of turbopumps, and the mass flow gain factor M is a rate of change in cavity volume for an oscillation of flow rate which is equivalent to an oscillation of an angle of attack. Although a measurement of the dynamic characteristics of cavitating turbopumps is not easy especially due to the difficulty in a precise measurement of the oscillating flow rate, our research group has succeeded in an acquisition of the reliable data of K and M for a turbopump inducer and it was found that the phase of oscillating cavity volume delays as the frequency increases [7]. Various types of cavitation such as a blade surface cavitation, a tip leakage vortex cavitation, and a backflow vortex cavitation occur at the same time in the inducer and the dynamic characteristics of each cavitation have not been experimentally clarified yet. Focusing on the blade surface cavitation as one of fundamental cavitation, we investigated the dynamic characteristics of the blade surface cavitation on a flat plate hydrofoil experimentally in the present study.

2. Dynamic Characteristics of the Blade Surface Cavitation on Hydrofoils

The continuity equation is represented as follows, using the oscillating volume flow rates at the upstream and down stream $\tilde{Q}_s$, $\tilde{Q}_d$, and the oscillating cavity volume $\tilde{V}_c$.

$$\tilde{Q}_d - \tilde{Q}_s = \frac{\mathrm{d}\tilde{V}_c}{\mathrm{d}t} \tag{1}$$

As $\tilde{V}_c$ can be thought to be a function of an inlet pressure and an angle of attack, a total differentiation of $\tilde{V}_c$ can be represented as follows:

$$\mathrm{d}\tilde{V}_c\left(\tilde{p}_s, \alpha\right) = \frac{\partial \tilde{V}_c}{\partial \tilde{p}_s}\mathrm{d}\tilde{p}_s + \frac{\partial \tilde{V}_c}{\partial \tilde{\alpha}}\mathrm{d}\tilde{\alpha} \tag{2}$$

Received November 3 2015; accepted for publication December 18 2015: Review conducted by Tadashi Tanuma, Ph. D. (Paper number O15064S)
Corresponding author: Hironori Horiguchi, Associate Professor, horiguti@me.es.osaka-u.ac.jp

This paper was presented at 13th Asian International Conference on Fluid Machinery (AICFM), September 7-10, 2015, Tokyo, Japan

From Eqs. (1) and (2), $\tilde{Q}_d - \tilde{Q}_s$ can be expressed as follows:

$$\tilde{Q}_d - \tilde{Q}_s = \frac{\partial \tilde{V}_c}{\partial \tilde{p}_s}\frac{\mathrm{d}\tilde{p}_s}{\mathrm{d}t} + \frac{\partial \tilde{V}_c}{\partial \tilde{\alpha}}\frac{\mathrm{d}\tilde{\alpha}}{\mathrm{d}t} \tag{3}$$

Assuming that the pressure and the angle of attack oscillate with a time dependence of $e^{i\omega t}$, the derivatives of the pressure and the angle of attack can be given by

$$\frac{\mathrm{d}\tilde{p}_s}{\mathrm{d}t} = i\omega\tilde{p}_s, \quad \frac{\mathrm{d}\tilde{\alpha}}{\mathrm{d}t} = i\omega\tilde{\alpha}. \tag{4}$$

Then, we define the non-dimensional angular velocity ω^*, the oscillating volume flow rate $\tilde{Q}^*$, the oscillating pressure $\tilde{p}^*$ and the oscillating cavity volume $\tilde{V}_c^*$ as follows:

$$\omega^* = \frac{\omega}{U/C}, \quad \tilde{Q}^* = \frac{\tilde{Q}}{CHU}, \quad \tilde{p}^* = \frac{\tilde{p}}{\rho U^2/2}, \quad \tilde{V}_c^* = \frac{\tilde{V}}{C^2 H}, \tag{5}$$

where *U*, *C*, *H*, and ρ represent a mean axial velocity in the test section, a chord length of the blade, a span of the blade, and a density of working fluid, respectively. The cavitation compliance *K* means a decreasing ratio of the cavity volume to the increase of the inlet pressure and the mass flow gain factor *M* means a increasing ratio of the cavity volume to the increase of the angle of attack, and they are defined as follows:

$$K = -\frac{\partial \tilde{V}_c^*}{\partial \tilde{p}_s^*}, \quad M = \frac{\partial \tilde{V}_c^*}{\partial \tilde{\alpha}}. \tag{6}$$

From Eqs. (4)~(6), Eq.(3) can be expressed as follows:

$$\tilde{Q}_d^* - \tilde{Q}_s^* = -i\omega^*(K\tilde{p}_s^* - M\tilde{\alpha}) \tag{7}$$

In the case with the excitation of the fluid and without the oscillation of the angle of attack ($\tilde{\alpha} = 0$), *K* is derived from Eq.(7) as follows:

$$K = -\frac{\tilde{Q}_d^* - \tilde{Q}_s^*}{i\omega^* \tilde{p}_s^*} \tag{8}$$

In the case without the excitation of the fluid and with the oscillation of the angle of attack, the pressure also oscillates. Therefore, *M* is derived from Eq.(7) as follows:

$$M = \frac{1}{\tilde{\alpha}}\left(K\tilde{p}_s^* + \frac{\tilde{Q}_d^* - \tilde{Q}_s^*}{i\omega^*}\right) \tag{9}$$

The value of *K* can be obtained by substituting the oscillating suction pressure and the oscillating volume flow rates measured in the case with the excitation of the fluid into Eq.(8). The value of *M* can be obtained by substituting the oscillating angle of attack, the value of *K*, oscillating suction pressure and oscillating volume flow rates measured in the case with oscillation of the angle of attack into Eq. (9).

3. The Experiment Setup and the Measurement of Oscillating Flow Rates

Figure 1 shows a schematic of the experimental facility used in the present study. Working fluid is deaerated water. A piston-type fluid exciter is installed in the upstream of a test section. Flow rates and the cavitation number $\sigma(=(p_{in}-p_v)/(0.5\rho v^2))$ are adjusted by a flow control valve and a vacuum pump, where p_{in} is an inlet pressure, p_v is a vapor pressure, ρ is a density of water, and *U* is a mean axial velocity. Pressures at positions 1-4 shown in Fig.1 were measured using differential pressure gauges (GE sensing, PMP5078), and used to evaluate the oscillating volume flow rate. Figure 2 shows a schematic of the test section. A sectional shape of the test section is a rectangle which is 70mm high and 100mm wide. The pressure p_{in} 120mm upstream of a leading edge of the hydrofoil was used as Eqs. (8) and (9).

Figure 3 shows a cross-section of the two-dimensional hydrofoil used in the present study. A suction side of the hydrofoil is flat. A chord length and a span of the hydrofoil are both 70mm. As shown in Fig.2, the hydrofoil is installed near the center of the test section with a tip clearance of 0.2mm. The hydrofoil can rotate around the center of the chord length. The oscillation of the angle of attack can be given by a D.C. motor through a link mechanism.

The oscillating volume flow rate was evaluated by the pressure difference between two points on the pipe in the present study. Considering a model of one-dimensional flow, a relation of oscillating flow velocities and pressures at two points of x_1 and x_2 is given as follows, based on the unsteady Bernoulli equation:

$$\frac{\tilde{p}_1 - \tilde{p}_2}{\rho} = \bar{u}_2\tilde{u}_2 - \bar{u}_1\tilde{u}_1 + \int_{x_1}^{x_2}\frac{dx}{A(x)}\frac{d\tilde{Q}}{dt}, \tag{10}$$

where *u* represents a flow velocity and superscripts of - and ~ represent mean and unsteady components. When the sectional area between two points on the pipe is constant and equals to *A*, Eq. (10) can be simplified as follows:

$$\frac{\tilde{p}_1 - \tilde{p}_2}{\rho} = \frac{x_2 - x_1}{A}\frac{d\tilde{Q}}{dt} \tag{11}$$

We assume that the unsteady components oscillate with a time dependence of $e^{i\omega t}$. Then, $\tilde{Q}$ can be represented by

$$\tilde{Q} = \frac{A}{\rho(x_2 - x_1)}\frac{\tilde{p}_1 - \tilde{p}_2}{i\omega}. \tag{12}$$

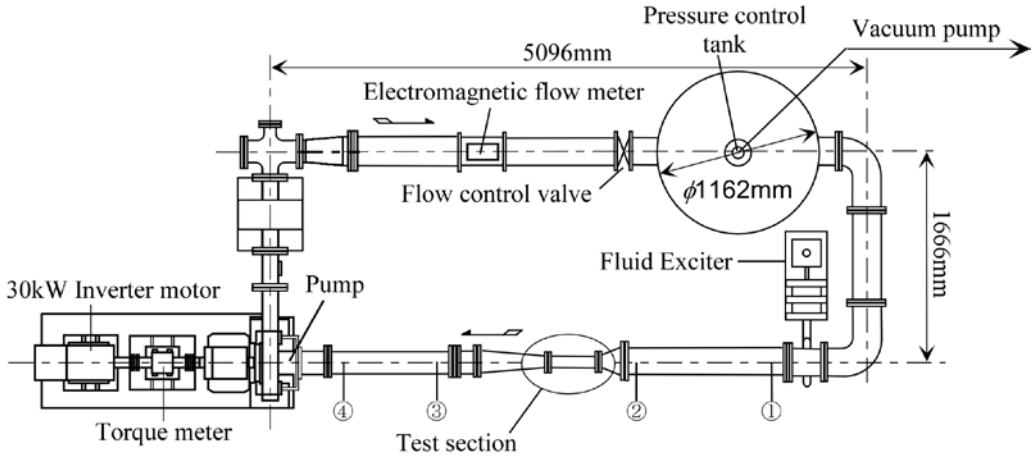

Fig. 1 The experimental facility

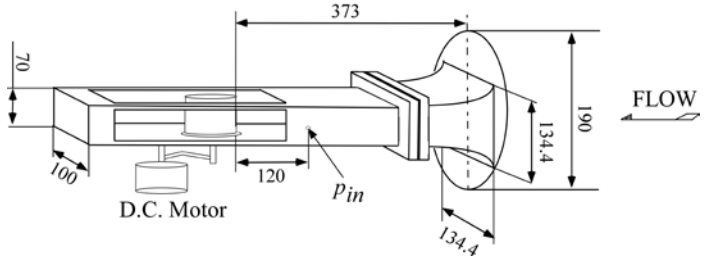

Fig. 2 The sketch of the test section

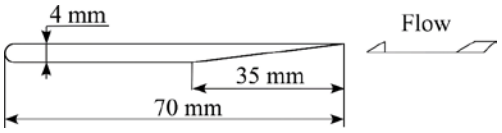

Fig. 3 The geometry of the flat plate hydrofoil

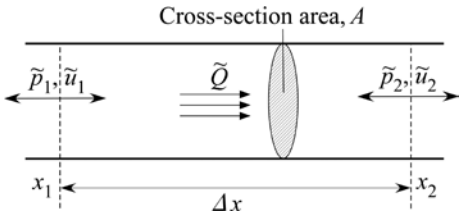

Fig. 4 The model of the one-dimensional flow

The oscillating flow rate $\tilde{Q}$ can be obtained by Eq. (12) through the use of the pressure difference $\tilde{p}_1 - \tilde{p}_2$.

The flow rates $\tilde{Q}_s$ and $\tilde{Q}_d$ in Eqs.(8) and (9) were evaluated by the pressure differences $\tilde{p}_1 - \tilde{p}_2$ and $\tilde{p}_3 - \tilde{p}_4$, respectively, where p_1, p_2, p_3 and p_4 were pressures at positions 1-4 shown in Fig.1.

4. Results and Discussion

4.1 Check of the Flow Conservation and Eigen Frequencies

The oscillating volume flow rates at the upstream and downstream sides of the hydrofoil have to be equal in non-cavitating conditions under a flow conservation law. To check the flow conservation, the flow was oscillated by the fluid exciter, and the upstream and downstream oscillating flow rates were measured in non-cavitating conditions. The oscillating flow rates were measured three times in each of conditions that the rotational speeds of the pump are 0rpm and 1500rpm, and those value were averaged. Figures 5(a) and (b) show the amplitude ratio $|\tilde{Q}_d / \tilde{Q}_s|$ of the oscillating flow rate and the phase $\mathrm{Arg}\left(\tilde{Q}_d / \tilde{Q}_s\right)$. As it was difficult to drive a piston of the fluid exciter sinusoidally at the quite low frequency of 1Hz, the experiment was conducted in frequencies more than 2Hz. From the equation of continuity, the amplitude ratio and the phase are theoretically equal to 1 and 0, respectively. The broken lines in Figs. 5(a) and (b) show the amplitude ratio, 1 and the phase, 0, respectively. The amplitude ratio and phase of $\tilde{Q}_d / \tilde{Q}_s$ in frequency ranges higher than 10Hz is more different from the theoretical value than that in frequency ranges lower than 10Hz. In lower frequency ranges, the amplitude ratios $\left|\tilde{Q}_d / \tilde{Q}_s\right|$ are within ±10% of the theoretical value and the phase $\mathrm{Arg}\left(\tilde{Q}_d / \tilde{Q}_s\right)$ are smaller than 2 deg.

Eigen frequencies around the test section were investigated by analyzing signals obtained from the differential pressure transducers installed in the upstream and downstream pipes by making an impact on the pipes. Figure 6 shows spectra obtained by

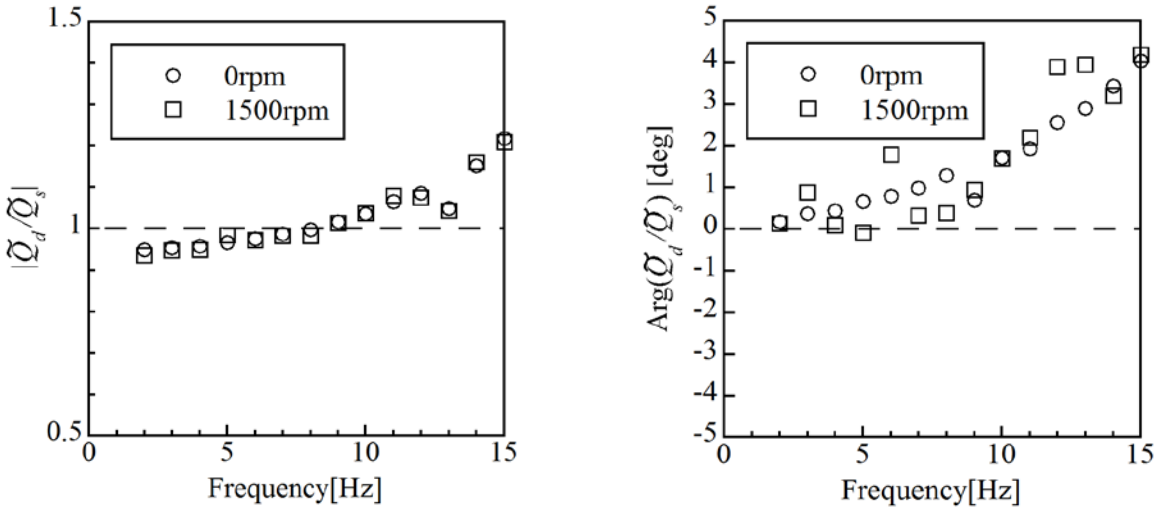

(a) Amplitude ratio (b) Phase

Fig. 5 The amplitude ratio and the phase of oscillating flow rates in the case with the excitation of the fluid

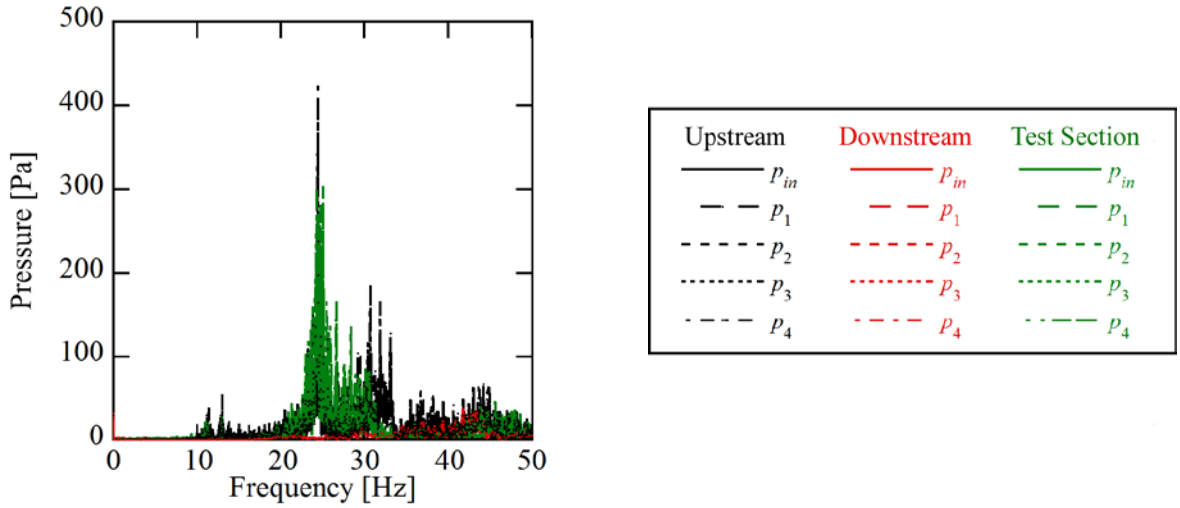

Fig. 6 Eigen frequencies of the test facility

FFT analysis of signals from the differential pressure transducers. Black, red and green lines in Fig. 6 show spectra obtained by making an impact on the upstream pipe, downstream pipe and a vicinity of the test section, respectively. In Fig. 6, we can confirm that there are few peaks of the pressure in frequency ranges lower than 10Hz and shape peaks of 24Hz appear in every cases.

Therefore, the experiment was conducted in frequency ranges from 2Hz to 10Hz where a flow conservation law was satisfied well comparatively, and a resonance of the system could be avoided.

4.2 The Cavity Length

Figure 7 shows the cavity length L/C against the cavitation number σ and $\sigma/(2\alpha)$ when the angle of attack α is 2deg. The cavity lengths were measured using pictures of the blade surface cavitation taken by the high speed camera. As the cavities were not uniform in a span direction due to the gravity, pictures of the cavity were taken five times in each condition and the lengths L of the cavity were measured at both ends and a center of the hydrofoil. The averaged values of them are shown in Fig. 7.

As shown in Fig. 7, the values of L/C increase with a decrease of σ. In the ranges of σ=0.6 - 0.8 ($\sigma/(2\alpha)$ = 8.6 - 11.46, L/C = 0.7 - 1.1), the distribution of L/C is not smooth and the values of L/C are larger than that of the fitted curve because the cavity was not stable due to the occurrence of a self-excited vibration of the cavity. The self-excited vibrations of the cavity whose length was longer than about 70% of the chord length has been observed in the experiment performed by Hashimoto et al [8]. Therefore, measurements of the dynamic characteristics were conducted in the ranges of $\sigma \geq 0.85$ ($\sigma/(2\alpha) \geq 12.18$) where the self-excited vibrations did not occur.

4.3 Observation of the Cavitation Using a High Speed Video Camera

The cavity was observed with a high speed video camera and the oscillating pressure $\tilde{p}_{in}^*$ was measured in the cases with the

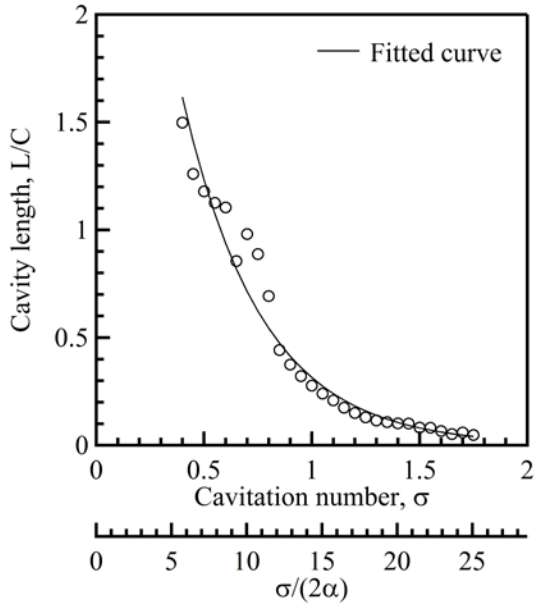

Fig. 7 The cavity length versus σ and $\sigma/(2\alpha)$. α=2.0deg

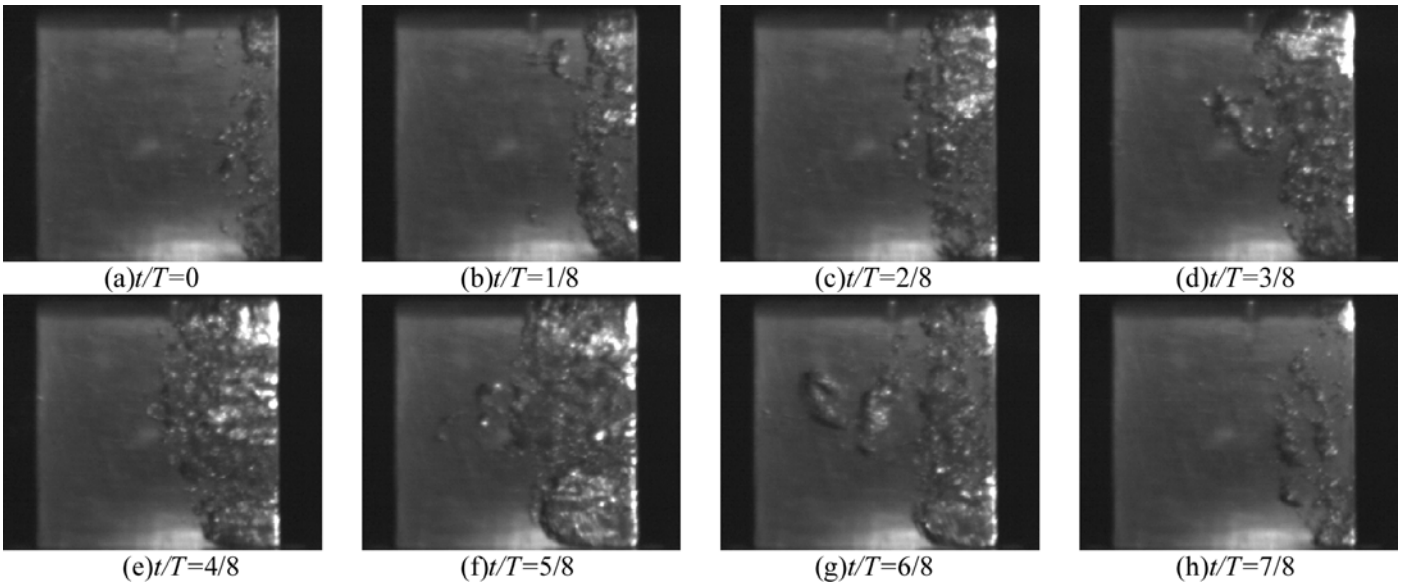

Fig. 8 Cavity shapes in the case with the excitation of the fluid at 9Hz and σ=0.95

excitation of the fluid and the oscillation of the angle of attack at 3, 6, 9Hz in four conditions of σ = 0.85, 0.90, 0.95, 1.00.

Figure 8 shows pictures of the cavity in the case with the excitation of the fluid at 9Hz and σ = 0.95. The pictures in every one-eight period were shown in Fig.8, where *T* means one period of the excitation of the fluid. *t*/*T* = 0 is the time when the suction pressure $\tilde{p}_{in}^{*}$ is maximum. As shown in Fig.8, longest cavity can be observed in *t*/*T*=4/8 - 5/8.

Figure 9 shows the non-dimensional cavity length *L*/*C* and the non-dimensional oscillating suction pressure $\tilde{p}_{in}^{*}$ in the case with the excitation of the fluid at σ =0.95. Figures 9(a), (b), (c) show results of the excitation of the fluid at 3Hz, 6Hz and 9Hz, respectively. As shown in Figs. 9(a), (b), (c), the cavity is longest near the time when $\tilde{p}_{in}^{*}$ is minimum. This tendency was observed at other cavitation numbers. Thus, it was found that the cavity responds to the inlet pressure $\tilde{p}_{in}^{*}$ with no phase delay.

Figure 10 shows pictures of the cavity in the case with the oscillation of the angle of attack ($\alpha = \bar{\alpha} + |\tilde{\alpha}|e^{i\omega t}$) of 3Hz at σ = 0.85. A mean angle of attack $\bar{\alpha}$ is 2deg and the amplitude of the angle of attack $|\tilde{\alpha}|$ is 0.5deg. The pictures in every one-eight period were shown in Fig.10, where *t*/*T* = 0 is the time when the oscillating angle of attack α is minimum and equal to 1.5deg. As shown in Fig.10, longest cavity can be observed in *t*/*T*=5/8 - 6/8.

Figure 11 shows time histories of the angle of attack, the non-dimensional cavity length *L*/*C* and the non-dimensional oscillating suction pressure $\tilde{p}_{in}^{*}$ in the case with the oscillation of the angle of attack at σ =0.85. Figure 11(a) shows a time history of the angle of attack. Figures 11(b), (c), (d) show results of the oscillation of the angle of attack of 3Hz, 6Hz and 9Hz, respectively. As shown in Figs. 11(b), (c), (d), a value of *t*/*T* when the cavity is longest decreases from *t*/*T*=0.7 to 0.6 with

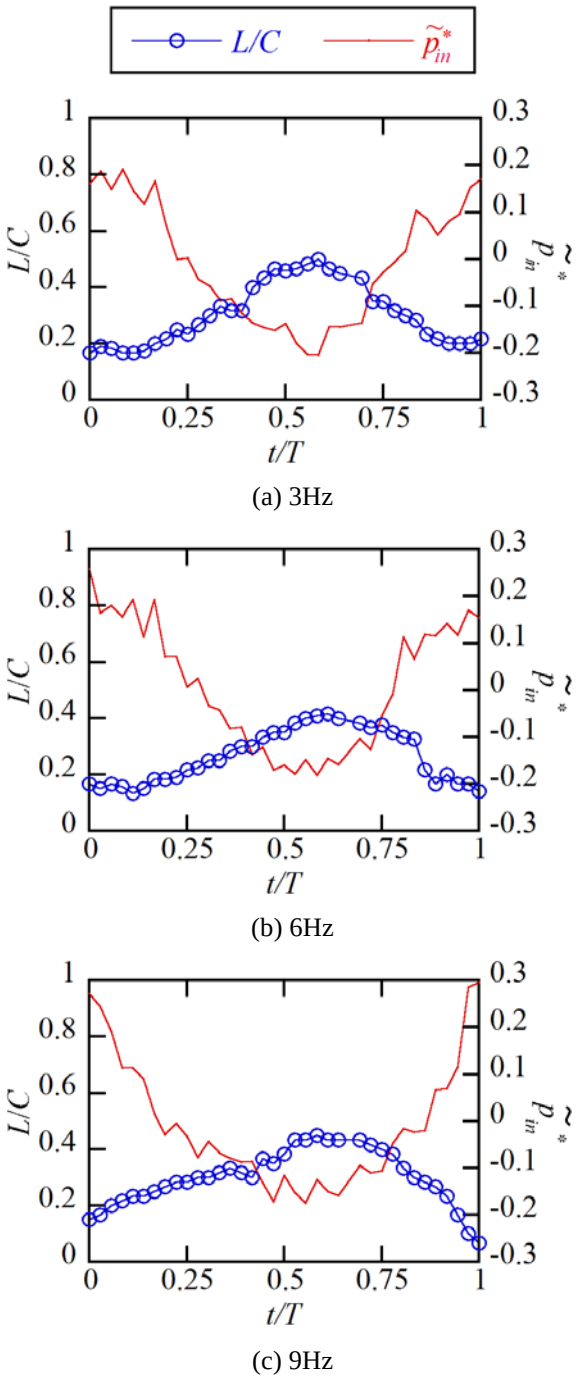

Fig. 9 The cavity length and the inlet pressure in one period in the case with the excitation of the fluid at σ=0.95

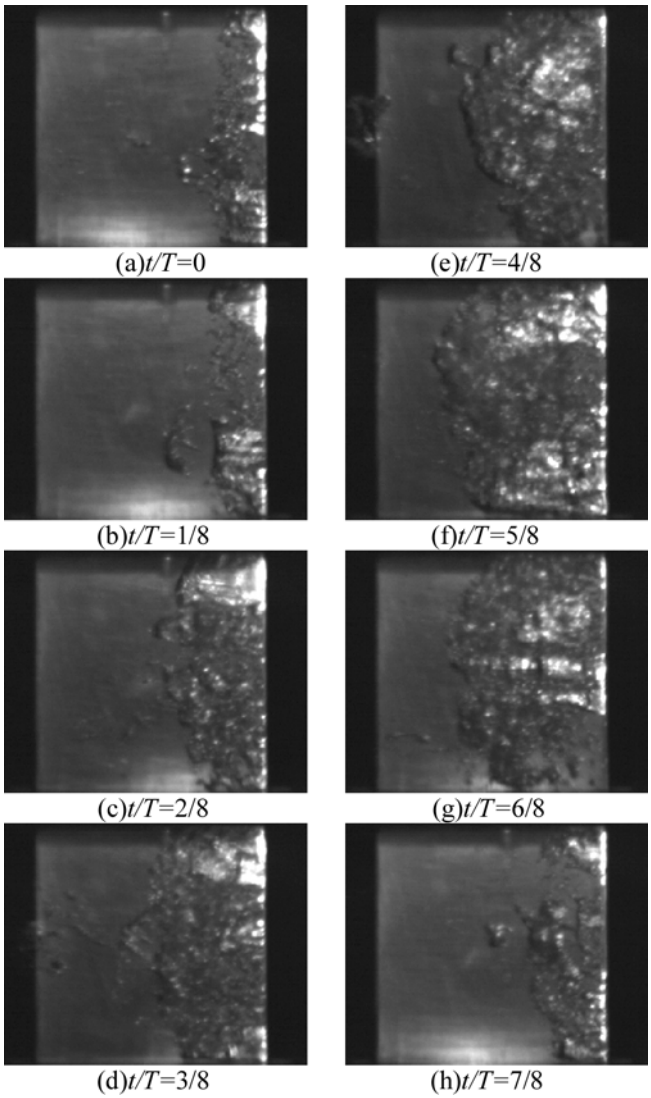

Fig. 10 The cavity shape in the case with the oscillation of the angle of attack at 3Hz and σ=0.85

increasing frequency. This tendency was observed at other cavitation numbers. Therefore, it was found that the cavity responds to the oscillation of the angle of attack with some phase delay and the phase delay decreases with increasing frequency.

4.4 Dynamic Characteristics of the Blade Surface Cavitation on the Flat Plate Hydrofoil

Figure 12 shows the cavitation compliance K and the mass flow gain factor M at a mean angle of attack $\bar{\alpha}$ =2.0 degrees and an amplitude of the angle of attack $|\tilde{\alpha}|$=0.5 degrees. The inlet pressure p_{in} in Fig. 2 was used as p_s in Eqs. (8) and (9). Figure 13 shows the amplitude and phase of K and M. The ranges of frequencies of K and M in Figs. 12 and 13 were from 4Hz to 10Hz because of reliabilities of the data.

Figure 13(a) shows that the amplitude of K decreases with increases of the frequency and the cavitation number. A volume of the cavity is smaller at larger cavitation number because the cavity is shorter and thinner. And, since a slope of the curve of the cavity length is smaller at larger cavitation number as shown in Fig. 7, the amplitude of the cavity volume can be smaller at larger cavitation number if we consider a quasi-steady change of the cavity. Therefore, it can be thought that the amplitude of K

decreases with increasing cavitation number. Figure 13(b) shows the phase of *K*. It was found that the phase of *K* is small and nearly equal to 0 especially at larger cavitation number. As shown in Figure 13(c), the amplitude of *M* slightly decreases with increasing frequency

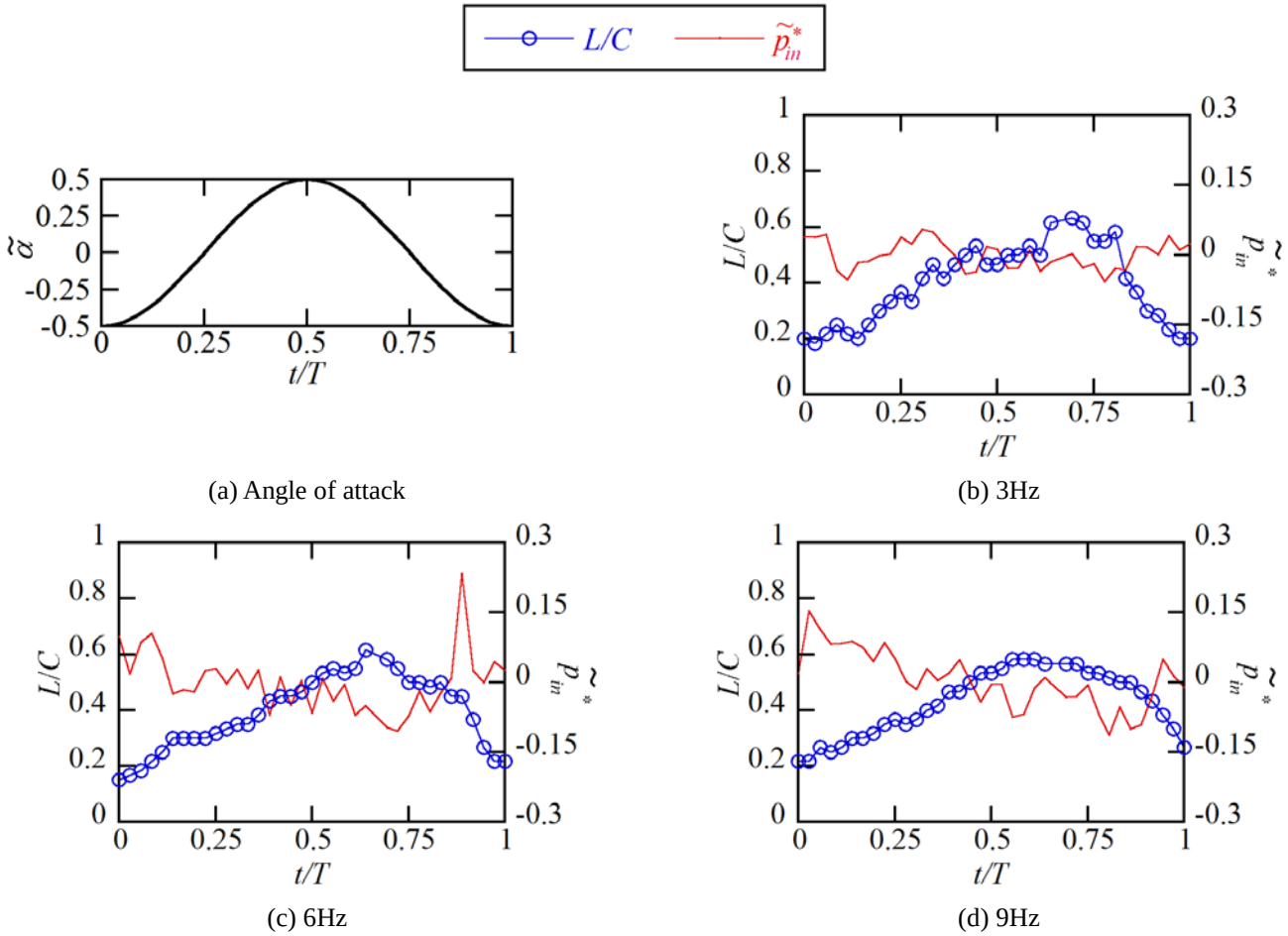

(a) Angle of attack (b) 3Hz

(c) 6Hz (d) 9Hz

Fig. 11 The angle of attack, the cavity length and the inlet pressure in one period in the case with the oscillation of the angle of attack at σ=0.85

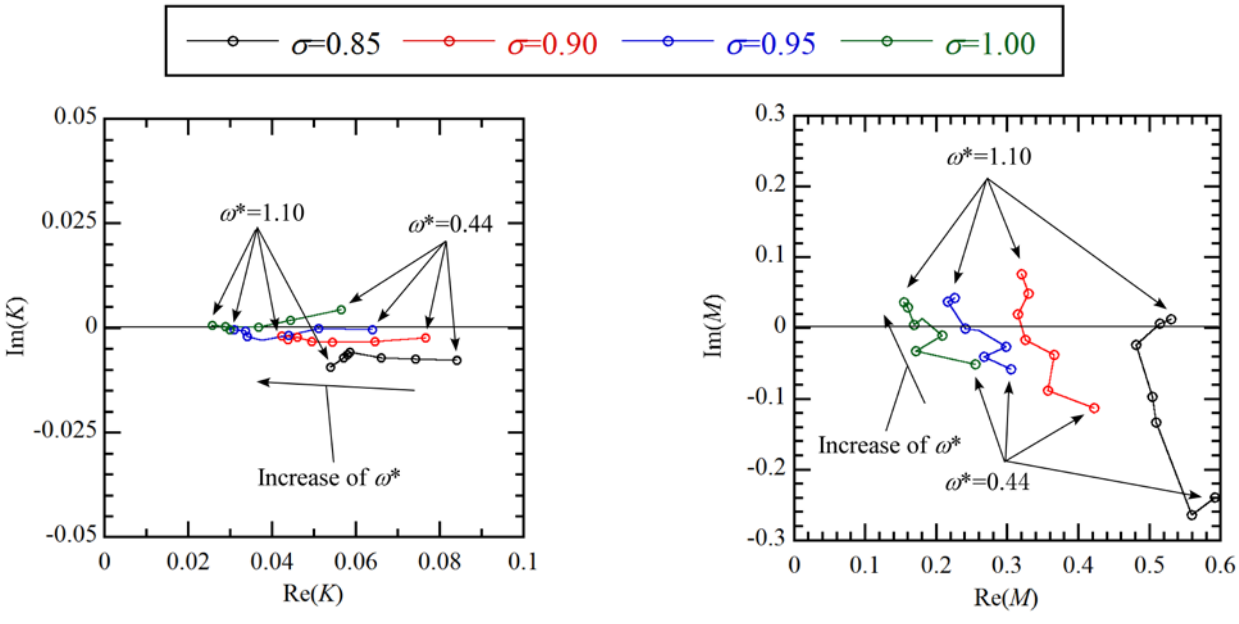

(a) *K* (b) *M*

Fig. 12 The cavitation compliance *K* and the mass flow gain factor *M*

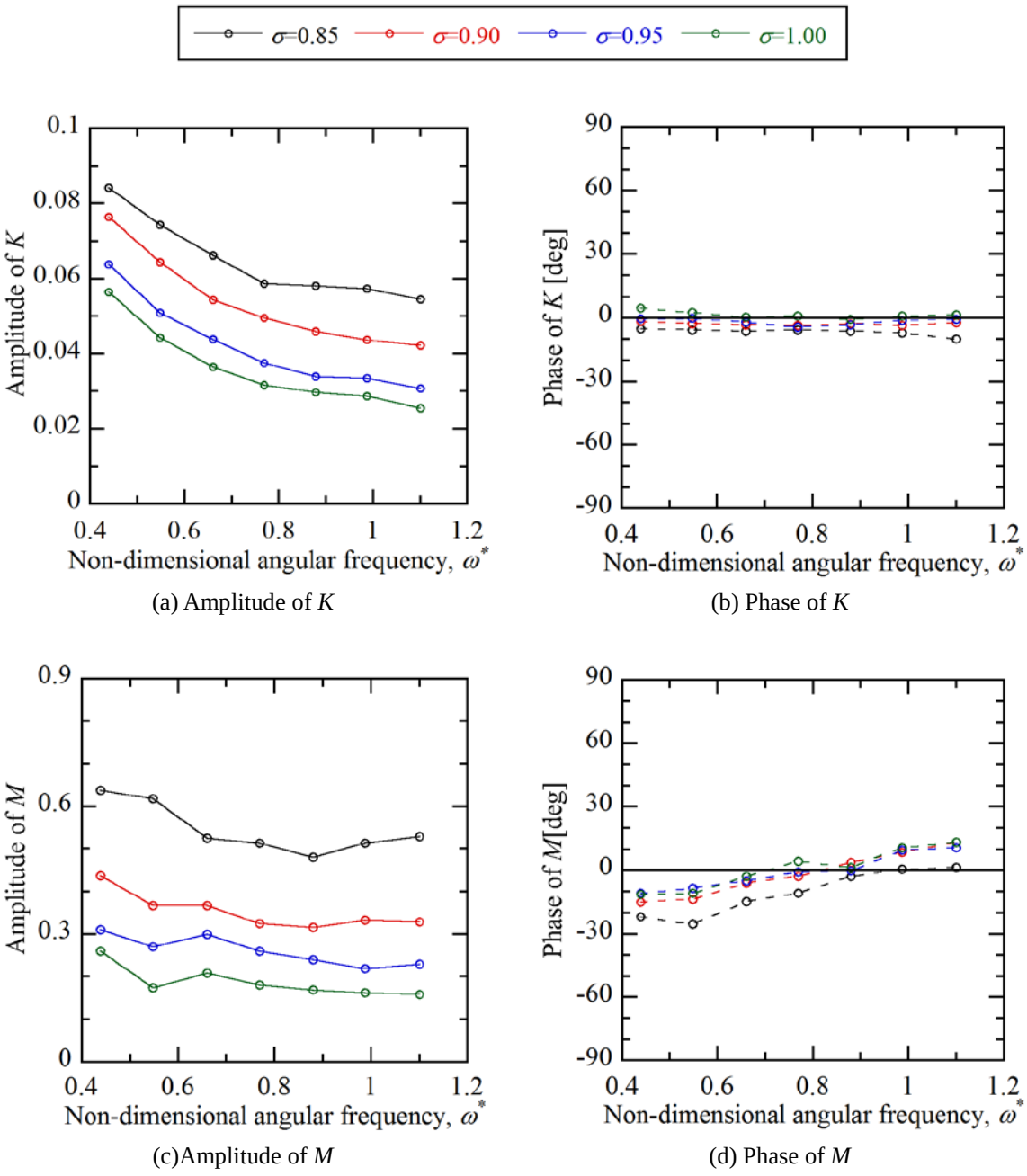

(a) Amplitude of *K*

(b) Phase of *K*

(c)Amplitude of *M*

(d) Phase of *M*

Fig. 13 The amplitude and the phase of *K* and *M*

and obviously decreases with increasing cavitation number. Figure 13(d) shows that the phase of *M* which is delayed in lower frequencies advances with increasing frequency and increases with increasing cavitation number.

5. Conclusion

Focusing on the blade surface cavitation as one of fundamental cavitation, we investigated the dynamic characteristics of the blade surface cavitation on a flat plate hydrofoil experimentally in the present study.

In an observation of the cavitation using a high speed video camera, unsteady characteristics of the blade surface cavitation were investigated and a validity of dynamic characteristics measured in the present study was confirmed. The dynamic characteristics of the blade surface cavitation are described below.

(1) The amplitude of the cavitation compliance decreases with increases of the frequency and the cavitation number.

(2) The phase of the cavitation compliance is small and nearly equal to 0 especially at larger cavitation number.

(3) The amplitude of the mass flow gain factor slightly decreases with increasing frequency and obviously decreases with increasing cavitation number.

(4) The phase of the mass flow gain factor which is delayed in lower frequencies advances with increasing frequency and increases with increasing cavitation number.

Acknowledgments

The present study was supported by JSPS KAKENHI Grant Number 26420112.

Nomenclature

C	Chord length	U	Average flow velocity in the test section
H	Span	V_c	Cavity volume
i	Imaginary unit	α	Angle of attack
K	Cavitation compliance ($=-\partial\tilde{V}_c^*/\partial\tilde{p}_s^*$)	ρ	Fluid density
L	Cavity length	σ	Cavitation number ($=(p_{in}-p_v)/(\rho U^2/2)$)
M	Mass flow gain factor ($=\partial\tilde{V}_c^*/\partial\tilde{\alpha}$)	ω^*	Non-dimensional angular frequency ($=\omega/(U/C)$)
p	Static pressure		
p_v	Vapor pressure	**Superscript**	
$\tilde{p}^*$	Non-dimensional oscillating pressure ($=p/(\rho U^2/2)$)	$\bar{}$	Mean component
		$\sim$	Unsteady component
Q	Volume flow rate	**Subscript**	
$\tilde{Q}^*$	Non-dimensional oscillating flow rate ($=\tilde{Q}/(CHU)$)	in	Inlet
		d	Discharge side
t	Time	s	Suction side
T	Period		

References

[1] Sack, L. E. and Nottage, H. B., 1965, “System Oscillations Associated With Cavitating Inducers,” Transactions of the ASME, Journal of Basic Engineering, Vol.87, pp.917-924.
[2] Miller, C. D. and Gross, L. A., 1967, “A Performance Investigation of an Eight-Inch Hubless Pump Inducer in Water and Liquid Nitrogen,” NASA TN D-3807.
[3] Acosta, A. J., 1958, “An Experimental Study of Cavitating Inducers,” Proceedings of the Second Symposium on Naval Hydrodynamics, ONC/ACR-38, pp.537-557.
[4] Kamijo, K., Shimura, T., and Watanabe, M., 1977, “An Experimental Investigation of Cavitating Inducer Instability,” ASME Paper 77-WA/FW-14.
[5] Tsujimoto, Y., Kamijo, K., and Brennen C. E., 2001, “Unified Treatment of Flow Instabilities of Turbomachines,” AIAA Journal of Propulsion and Power, Vol.17, No.3, pp.636-643.
[6] Brennen, C. E. and Acosta, A. J., 1973, “Theoretical, Quasi-Static Analysis of Cavitation Compliance in Turbopumps,” AIAA Journal of Spacecraft and Rockets, Vol.10, No.3, pp.175-180.
[7] Ashida, T., Yamamoto, K., Yonezawa, K., Horiguchi, H., Kawata, Y., and Tsujimoto, Y., 2014, “Measurement of Dynamic Characteristics of an Inducer in Cavitating Conditions (in Japanese),” Turbomachinery, Vol.42, No.10, pp.642-654.
[8] Hashimoto, A., Watanabe, S., Asahara, T., Sato, K., and Tsujimoto, Y., 2001, “Unsteady Characteristics of Cavitation on an Oscillating Hydrofoil (1st Report, Experimental Observation of Cavity Behavior) (in Japanese),” Transactions of the JSME, Series B, Vol.67, No.654, pp.391-397.